Design of a 45 kW Permanent Magnet Synchronous Motor for a Hybrid Electric Vehicle

St. Henneberger, S. Van Haute, K. Hameyer and R. Belmans

Katholieke Universiteit Leuven
E.E. Dept., Div. ESAT/ELEN
Kardinaal Mercierlaan 94, B-3001 Leuven - Heverlee, Belgium

Abstract - In the framework of the development of a drive system for the implementation in a hybrid electric vehicle, a 45 kW 6-pole permanent magnet synchronous motor (PMSM) is designed. The aims of the drive development and the design methods are discussed. The design takes advantages of analytical calculations as well as static Finite Element Analysis.

1. INTRODUCTION

The requirements for a motor designed for an electric vehicle are multiple: high efficiency, large field weakening range, high power/weight ratio and high reliability. Furthermore, the motor has to fulfill economic requirements and has to provide a certain level of comfort concerning noise and smooth operation.

Hybrid electric vehicles have the advantage to operate with zero emission in the inner city while not being limited in the range for intercity distances. In further, the possibility of regenerating the breaking energy is offered. The aim is the development of a vehicle that can be used in public transport as well as in different delivery systems. A tourist bus should be able to transport up to fifteen persons through a town slowly, but with a maximum of comfort. A city taxi has to carry six people within a city, being able to follow the normal traffic flow. The delivery systems can be split into two groups. The mail delivery prefers the normal speed of the city traffic, whereas for the customer delivery the transport capacity is more important.

2. HYBRID ELECTRIC DRIVE

The main parts of the drive equipment are the energy sources, in this study a Diesel generator connected in parallel to a rechargeable NiCd traction battery, the traction motor with converter and controller, and the main controller unit. The drive module is connected to a main controller collecting the status information: acceleration, deceleration, regenerating the breaking energy, etc. (Fig. 1). The desired torque T_d given by the driver of the vehicle is processed by the main controller.

The requirements of the traction motor are summarised in table 1, stressing the limit of the total weight to be G_{mot} = 60 kg.

Tab. 1 Design demands on the traction motor

Rated power	45 kW
Rated torque	187 Nm
Rated speed	2300 rpm
Maximum weight	60 kg
Efficiency	95 %

The heart of the drive-train consists of the permanent magnet excited synchronous machine. In the past variable speed drives have been dominated by dc machines. This is due to its simple control structure and the low converter expenses. With ongoing developments in power electronics and their components, regarding possibilities and the price as well, the conventional dc machine is partially substituted by three phase induction motors and permanent magnet excited servo machines. With the developments in rare earth permanent magnet technologies, the inset of high energy and high quality motors with a low ratio of weight to volume is possible.

The separately excited dc motor with mechanical commutator is widely used on the account of its good dynamic and static behaviour. However, its application is limited to speeds below 10,000 rpm. In order to achieve a high speed drive to reduce volume and weight at the same output power, it is necessary to replace the mechanical commutator by an electronic one. An electronically commutated machine offers the advantage of a long lifetime, low maintenance, low audible noise, wide speed range, easy speed control, high pull out torque, high efficiency and suitability under extreme conditions. The basic failure rate of brushless motors is much lower compared to motors with brushes.

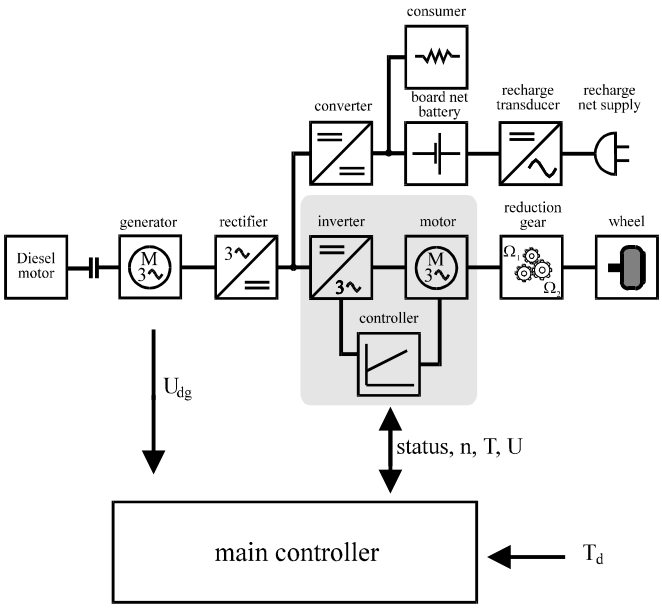

Fig. 1 Topology of the hybrid drive concept.

In the brushless type of motor the armature winding is transferred to the stator and the exciting field winding is replaced by a permanent magnet system in the rotor.

Due to the absence of losses generated in the exciting field winding the high efficiency of the permanent magnet synchronous machine (brushless ac machine), makes this type of motor advantageous for application supplied by batteries. In recent years the permanent magnet brushless dc motor has been the first choice in drive systems for electric vehicles. The brushless ac motor however seems to become the standard in the next few years.

In a brushless ac motor the terminal current is sinusoidal. Depending on the individual rotor construction, the shape of the rotor field can mainly be found in a block shape. Using a distributed three phase stator winding, the induced voltage becomes sinusoidal. Therefore, the machine generates a time and position independent constant torque. Due to a lower content of harmonics in the air gap field when compared to the brushless dc motor, values of efficiency are increasing. Furthermore, less torque ripple and audible noise are generated. However, a much more precise and expensive position sensor is required to control the machine behaviour.

3. ADVANCED FIELD WEAKENING

The wide speed range (rated speed of 2300 rpm, maximum speed of 7300 rpm) is obtained by applying advanced field weakening techniques. Therefore, the rotor requires a magnetically asymmetrical design (Fig. 2) and an adapted control strategy [1]. In the constant torque zone the drive speeds up by raising the stator frequency and voltage until rated speed is reached. To increase speed further, power and voltage stay constant while increasing the angle between stator current and field axis above 90º by additionally applying a negative direct stator current component (Fig. 3). Consequently the required current is minimised and the possibility of demagnetising the magnets irreversibly is reduced.

The significant saliency of the motor, realised by constructing a rotor with surface-inset magnets (Fig. 2), produces a reluctance torque.

A further benefit of the surface inset structure is that the torque, exerting forces on the magnets, is transferred to the rotor core by the iron in the rotor pole gap [4]. Furthermore the rotor surface can be smooth being rather important for the mechanical banding. A disadvantage of this surface-inset type is an increased flux. Also a higher torque ripple is caused by the saliency.

The equation, describing the torque, is a function of the angle $\Psi = 90º-\delta$, which describes the advanced field weakening and can be splitted into an electromagnetic component

$$T_e(\Psi) = \frac{3 \cdot p}{\omega_0} \cdot E \cdot I_q \qquad (1)$$

and a reluctance component,

$$T_r(\Psi) = 3 \cdot p \cdot I_d \cdot I_q \cdot (L_q - L_d) \qquad (2)$$

With $I_d = I \cdot \sin(\Psi)$ and $I_q = I \cdot \cos(\Psi)$.

The optimum rotor torque angle for the maximum torque $T = T_e+T_r$ is expressed by the equation

$$\Psi_{opt} = a\sin\left(\frac{E}{4 \cdot I_1 \cdot (X_q - X_d)} - \sqrt{\left(\frac{E}{4 \cdot I_1 \cdot (X_q - X_d)} \right)^2 + \frac{1}{2}} \right) . (3)$$

4. MOTOR DESIGN

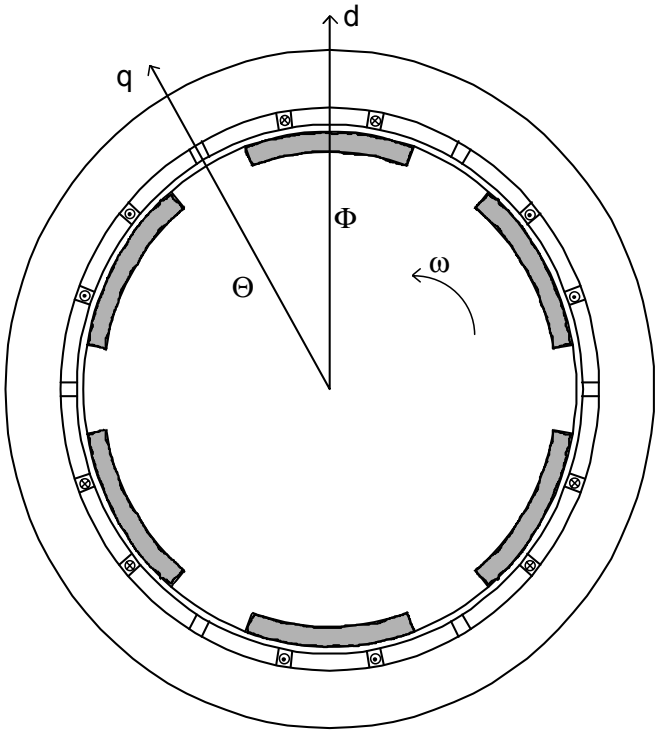

Fig. 2 Cross-sectional view a of 6-pole PMSM. The q- and the d-axis are indicated.

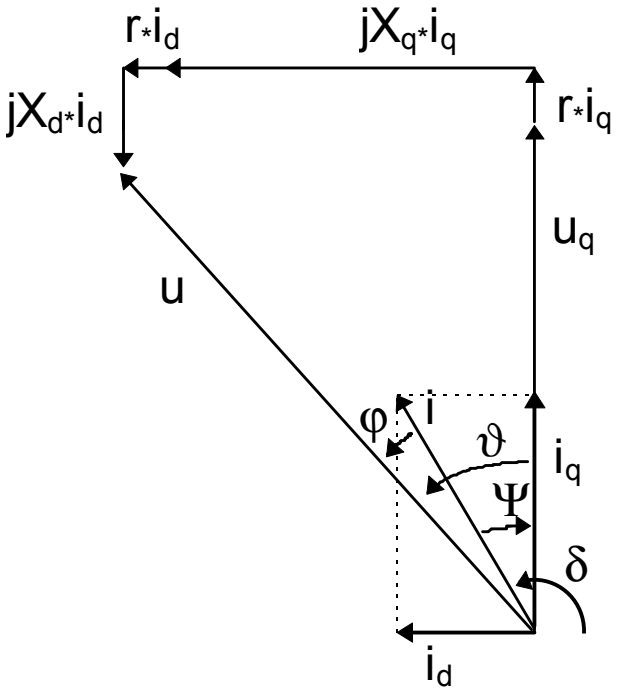

Fig. 3 Phasor diagram of the PMSM in the advanced field weakening mode.

A. Design methods

In a first step the motor is designed by an analytical approach being based on the generalised electric machine theory [2], [3]. A PMSM can be modelled by mathematical equations subject to the following assumptions:

- Ferromagnetic materials have an infinite permeability.
- Tooth and slot effects can be adequately accounted for by Carter's Coefficient [1].

Thus, the analytical calculation contains a lot of empirical formulations which have to be checked by a numerical field analysis. When a motor model is found, the necessary data are created to start a finite element computation. The FEM is an accurate method for electromagnetic field calculations, since it takes into account the non-linearity of all ferro magnetic materials, the detailed rotor and stator structure and the distribution of the stator windings. More than one finite element solution is required in order to find the motor parameters that have to be checked. In order to evaluate the steady state torque, as found from the analytical solution, only one solution is required. If the torque ripple is to be assessed, the solution must be repeated for multiple rotor positions. The magnets have to be checked against demagnetisation as well. This can be done by supplying the transient short circuit current to the model and by evaluating the demagnetisation in the model. From two solutions, the d- and q-axis inductances are found.

B. Design aspects

In order to achieve a high efficiency of the PMSM the losses have to be kept low being contrary to a high power/weight ratio. Therefore, the optimal choice of a desired low weight and acceptable iron losses has to be done. In the same way, the contributing losses can be reduced by using more winding copper, yielding in increasing costs and additional weight. Iron losses are decreased by choosing thin low-loss lamination in the stack of the stator. The power/weight ratio is further improved by applying an indirect water-cooling system.

The thickness of the iron joke applying a high number of poles. However, the number of poles is limited by the frequency of the inverter, and furthermore, a wide range of field weakening can only be achieved by a small number of poles.

Neglecting the stator resistance, the field weakening range is described by the equation

$$\frac{n_{max}}{n_0} = \frac{1}{1 - i_d \cdot x_d} . \qquad (4)$$

Increasing X_d by decreasing the thickness of the permanent magnets has limits. It enables their demagnetisation and reduces the reluctance torque by diminishing the ratio X_q/X_d.

Half closed slots reduce the slot harmonics which are responsible for iron losses and eddy current losses in the permanent magnets. However, due to the relatively large effective air gap caused by the magnets, the opening of the stator slots are kept wide, avoiding that the flux forced by the current closes in the stator iron without passing the air gap.

Another design aspect is the choice of the permanent magnet material. A high remanent flux density is needed, while a high coercivity is less important as overloads do not occur. NdFeB permanent magnets offer a high energy density as well as a high remanence flux density. Furthermore, the operating high temperatures are no longer a drawback as the new generation of NdFeB magnets (VACODYM 411) retains its magnetic properties up to high temperatures of 120º C.

Using surface mounted magnet pieces, glued onto the rotor, instead of one magnet piece for one pole, reduces eddy current losses and herewith the heating up of the magnets.

C. Machine data

The analytical calculation results in the following data: Machine dimensions, computed parameters and electric quantities at rated load:

Tab. 2a Dimensions of the PMSM

Stack OD	299 mm
Stack ID	208 mm
Rotor length	130 mm
Overall mass	60.4 kg
Air gap length	1 mm
Thickness PM	3 mm
Angular magnet width	63 º
Number of poles	6

Tab. 2b Parameter of the PMSM

Stator resistance	9.5 mΩ
Inductance d-axes	0.50 mH
Inductance q-axes	0.72 mH
Rotor inertia	0.18 kgm^2

Tab. 2c Electric quantities of the PMSM

emf	64.8 V
Voltage d-axes	-101.8 V
Voltage q-axes	38.3 V
Terminal voltage	108.5 V
Rated current	208.8 A
Rated speed	2298
Output power	44.6 kW
Mechanical torque	186 Nm

The motor from table 2 fulfills the requirements. The high efficiency at partial load is shown by calculating the operating points of the equivalent circuit of the machine. The speed, the output power and mechanical torque are calculated as function of the supplied voltage at rated current. The rotor torque angle δ_{opt} is constant until rated speed is reached, then the current component of the d-axes increases by enlarging the rotor torque angle δ (Tab. 3). The results of table 3 are plotted in a diagram (Fig. 4).

Tab. 3 Stationary operating points as function of the voltage and the rotor torque angle δ.

U	n	I	T_m	P_m	Ψ	η

	[rpm]	[A]	[Nm]	[kW]	[°]	[%]
0.2*U_n	436	208.8	186.17	8.50	-112.2	86.80
0.4*U_n	902	208.8	185.97	17.57	-112.2	92.78
0.6*U_n	1368	208.8	185.76	26.60	-112.2	93.99
0.8*U_n	1833	208.8	185.56	35.62	-112.2	94.79
1.0*U_n	2299	208.8	185.36	44.62	-112.2	95.76
1.0*U_n	2633	208.8	179.52	49.51	-123.8	96.30
1.0*U_n	3147	208.8	161.38	53.64	-135.3	96.57
1.0*U_n	4124	208.8	131.25	56.69	-146.9	96.70
1.0*U_n	6648	192.65	81.46	56.71	-158.4	96.23
1.0*U_n	7331	181.37	72.01	55.28	-159.4	96.12

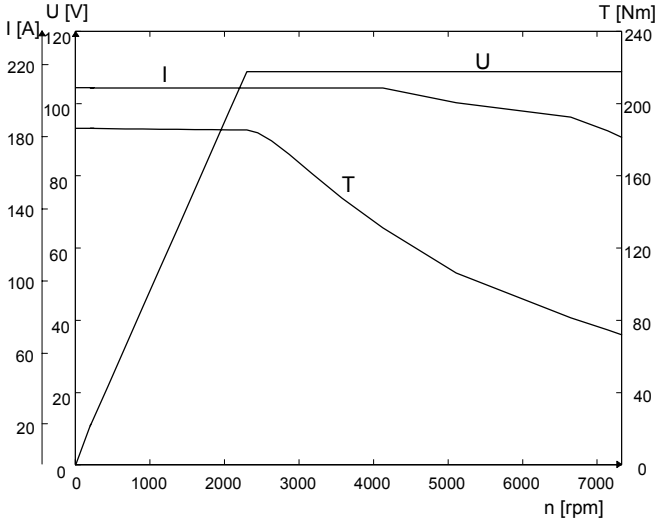

Fig. 4 Voltage, current and mechanical torque as function of the speed.

5. NUMERICAL CALCULATIONS

The results of the analytical approach have to be checked by numerical field analysis. The electromagnetic torque is computed by the Maxwell stress tensor and the inductances are derived by using the stored magnetic energy. Furthermore, the magnetic flux density is check for saturation values, the Carter factor is calculated and adapted in the analytical program and the generated torque ripple is analysed. Fig. 5 shows the flux plot of one pole of the motor operating under rated condition, indicating the maximum flux density in the stator teeth, the stator yoke and in the rotor yoke.

The torque is calculated as function of the rotor torque angle δ at rated current. Fig. 6 shows the numerical computation compared with the analytical calculation. If advanced field weakening is not applied ($\delta = 90°$), meaning that the torque only consists out of a electromagnetic component, the error between the two results is less than 3 % ($T_{ana}(\delta = 90°) = 165.9$ Nm; $T_{num}(\delta = 90°) = 161.2$ Nm).

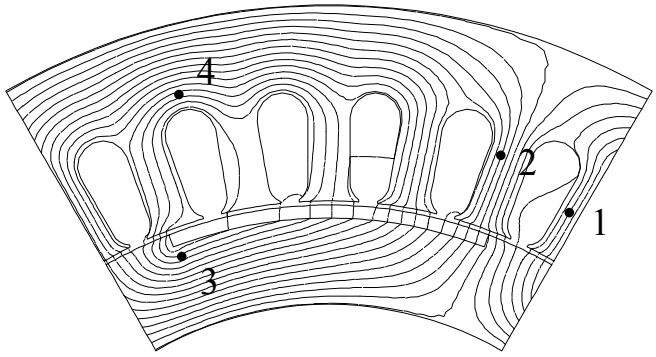

Fig. 5 Flux plot of one pole at rated working condition.
$B_1 = 1.95$ T; $B_2 = 1.85$ T; $B_3 = 1.98$ T; $B_4 = 1.90$ T

The difference in the results of the analytical and the numerical calculation appears if advanced field weakening is applied. The maximum torque is obtained for different rotor torque angles ($T_{ana}(\delta = 112°) = 185.4$ Nm; $T_{num}(\delta = 125°) = 187.3$ Nm).

The calculation of the reluctance component of the torque (Fig. 7) confirms that the reason for the difference of the two curves of Fig. 6 has to be found in the determination of the inductances.

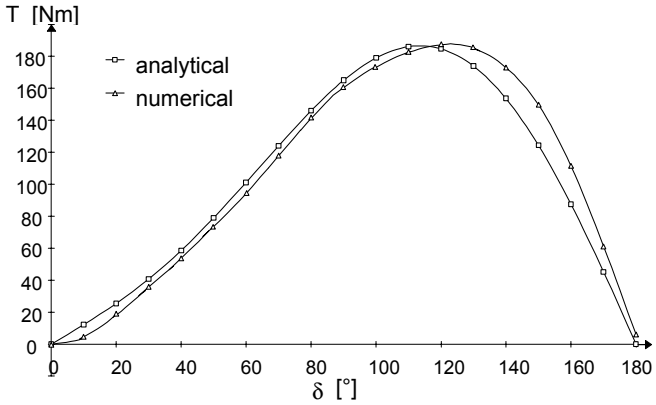

Fig. 6 Analytical and numerical computation of the torque as function of the rotor torque angle.

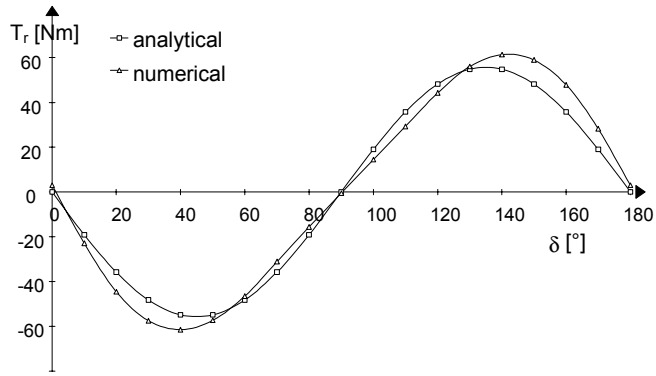

Fig. 7 Analytical and numerical computation of the reluctance torque as function of the rotor torque angle.

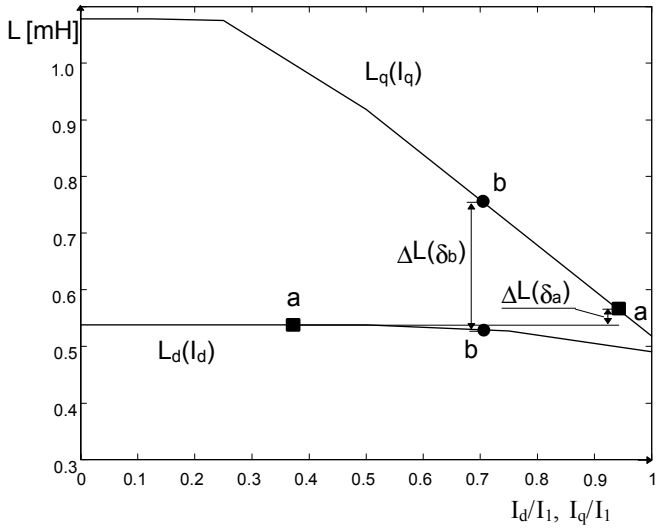

Fig. 8 Analytical and numerical computation of the reluctance torque as function of the rotor torque angle.

Due to saturation effects in the stator teeth and the iron in the rotor pole gap the inductances are a function of the current as well as the rotor torque angle. Fig. 8 shows the difference $\Delta L = L_q - L_d$ for two rotor torque angles δ_a and δ_b. ΔL rises if δ increases, because L_d is becoming slightly saturated while L_q becomes unsaturated. Therefore, the varying inductances L_d (I,δ) and L_d (I,δ) have to be adapted to the control algorithm.

6 CONTROL

Regarding the additional reluctance torque, the control algorithm has at any instant to determine the optimum torque per Ampere trajectory [1]. The transition between constant torque and constant power region should be smooth. Several algorithms for flux weakening have been published recently [4], [6]. A general flux weakening algorithm is adapted to the designed 45 kW motor and implemented on a DSP based hardware system. It applies negative direct-axis currents over the entire speed region, taking advantage of the asymmetrical rotor construction. The optimum angle δ is determined for operating points both, in the constant torque region as well as in the constant power region.

Fig. 9 shows the control system. It meanly consists out of a controller board with additional I/O features and an encoder interface, a host PC, an IGBT inverter, current sensors and an incremental encoder. The dotted frame indicates the functions that are implemented on the controller board.

The heart of the controller board is a TMS320C31 Digital Signal Processor with a 40 Mhz clock rate and 50 ns cycle time. A slave processor is used to perform the digital input and output and to generate the PWM signals. The inverter used is a slightly modified standard VSI-PWM inverter with IGBTs. The high switching rate of the power electronic components is important, especially when a PMSM with sinusoidal waveforms is considered. When switching frequencies up to 20 kHz are available, the audible noise level can be reduced substantially.

Motor currents are measured and fed to the control board by 16 bit AD converters and are digitally filtered. The position is measured using an incremental encoder. The signals are directly connected to the encoder interface on the controller board. In this way, an expensive resolver for continuous position sensing is avoided. The disadvantage using an encoder will be overcome in future implementations by sensorless operation of the drive.

The direct and quadrature axis current components are calculated by the Parks transformation and are apllied to the control algorithm. The algorithm determines reference values for the direct and quadrature axis currents. The implemented PWM generation scheme in the slave processor is based on phase voltage reference values. For this reason, these reference values are determined using a decoupling network and the inverse Park transformation. For an electric vehicle application, the use of classical PI-controllers in the decoupling system is satisfying [6].

Because of the presence of a varying dc-bus voltage (battery voltage 240 V to 400V), it is also measured and used in the outer voltage control loop of the control algorithm to determine the point of transition from the constant torque to the constant power region [9].

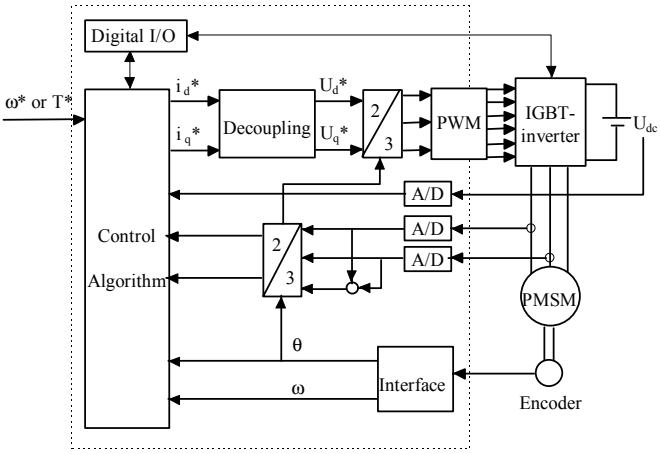

Fig. 9 Control system for the PMSM

6 CONCLUSIONS

In this paper the design of a PMSM for a hybrid electric vehicle has been presented. The aim to get a high efficiency and a high power/weight ratio has been reached by minimising all kinds of losses and applying advanced field weakening techniques. A large field weakening range has been realised. Apart from the optimum rotor torque angle, the analytical design and to the numerical calculations are in good agreement. The varying inductances are considered in the adapted control strategy.

LIST OF SYMBOLS

emf	E	voltage d/q-axes	$U_{d/q}$

torque	T	current d/q-axes	$I_{d/q}$
electromagnetic torque	T_e	inductance d/q-axes	$L_{d/q}$
reluctance torque	T_r	rotor torque angle	δ
rated speed	n_0	angle between E and I	ψ

ACKNOWLEDGEMENTS

The authors are indebted to the Belgian Ministry of Scientific Research for granting the project IUAP No. 51 on Magnetic Fields. Furthermore, the research is supported by Flanders' Secretary of Economy.

REFERENCES

[1] Nasar, S. A., Boldea, I., Unnewehr, L. E.: "Permanent Magnet, Reluctance, and Self-Synchronous Motors". CRC Press, 1993, London Tokyo

[2] L. Chang, G. E. Dawson, T. R. Eastham; "Permanent Magnet Synchronous Motor Design: Finite Element and Analytical Methods"; ICEM Conf. Proceedings, Cambridge, pp. 1082-1088, Aug. 1990.

[3] Slemon, G. R.: Xian, L.: "Modelling and Design Optimisation of Permanent Magnet Motors". Electric Machines and Power Systems, vol. 20, no. 2, pp. 71-92, April 1992.

[4] Nipp, E.: "Alternative to Field Weakening of Surface Mounted Permanent Magnet Motors for Variable Speed Drives". Proc. IAS'95, pp. 191-198.

[5] Sebastian T., Slemon, G. R., Rahman, M. A.: "Design Considerations for Variable Speed Permanent Magnet Motors", Proc. ICEM'86, part 3, pp. 1099-1102, Munich, Sept. 1986.

[6] Kim, J.-M. Sul S.-K.: "Speed Control of Permanent Magnet Synchronous Motor Drive for Flux Weakening Operations". Proc. IAS'95, pp. 216-211.

[7] Henneberger G., Hadji-Minaglou J.-R., Ciorba R. C. ; "Flux-Weakening Operations of Permanent Magnet Synchronous Motors for Electric vehicle Operation"; Workshop on Electric and Magnetic Fields, Leuven, Conf. Proceedings, pp. 57-60, May 1994.

[8] Ghribi M., Le-Huy H., "Optimal Control and Variable Structure Combination Using a Permanent Magnet Synchronous Motor", IAS Conf. Proceedings, Denver, pp. 408-415, Oct. 1994.

[9] Hadji-Minaglou J.-R: "Antriebskonzepte mit permanent-erregten Synchronmotoren für den einsatz im Elektrofahrzeug", PhD-thesis RWTH Aachen, jul. 1994.